Chapter 17
Jahn-Teller Transitions in the Fe(II)Fe(III) Bimetallic Oxalates

R.S. Fishman

Abstract Because the orbital angular momentum L_z^{cf} on the Fe(II) sites of the Fe(II)Fe(III) bimetallic oxalates is incompletely quenched by the crystal field, the spin-orbit coupling competes with the Jahn-Teller (JT) distortion energy. The value of L_z^{cf} depends on the cation between the bimetallic layers. When L_z^{cf} is sufficiently small, the open honeycomb lattice of each bimetallic layer is distorted at all temperatures below the JT transition temperature. But in a range of L_z^{cf}, the lattice is only distorted between lower and upper JT transition temperatures, $T_{\rm JT}^{(l)}$ and $T_{\rm JT}^{(u)}$. For some cations, L_z^{cf} may exceed the threshold required for the cancellation of the moments on the Fe(II) and Fe(III) sublattices at a temperature T_{comp} below the transition temperature T_c. Using elastic constants obtained from compounds that exhibit magnetic compensation, we find that $T_{\rm JT}^{(l)}$ always lies between T_{comp} and T_c and that $T_{\rm JT}^{(u)}$ always lies above T_c.

17.1 Introduction

With their low density, multifaceted functionality, and possible biocompatibility, molecule-based magnets have attracted great attention over the past two decades [1]. Like conventional solid-state magnets, bulk molecule-based magnets are typically crystalline with an extensive number of magnetic ions. The building blocks of molecule-based systems are organic molecules but the magnetic species may be either transition-metal ions or organic radicals. Unlike in conventional magnets, the competing spin-orbit, crystal-field, and exchange energies in a molecule-based

R.S. Fishman (✉)
Materials Science and Technology Division, Oak Ridge National Laboratory, Oak Ridge, TN 37831-6065, USA
e-mail: fishmanrs@ornl.gov

M. Atanasov et al. (eds.), *Vibronic Interactions and the Jahn-Teller Effect: Theory and Applications*, Progress in Theoretical Chemistry and Physics 23,
DOI 10.1007/978-94-007-2384-9_17,

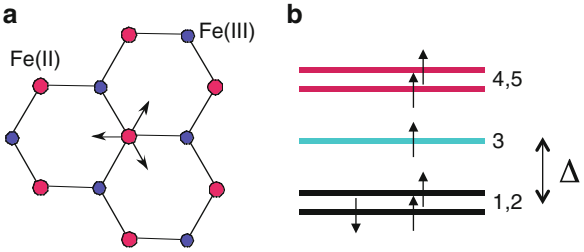

Fig. 17.1 (**a**) A portion of the open honeycomb lattice, displaying the three possible displacements of an Fe(II) ion into adjacent hexagons. (**b**) Level-splitting of the $3d^6$ Fe(II) multiplet in a C_3-symmetric crystal-field

magnet can be tuned by the choice of organic cation or by applying pressure. These competing energies produce a remarkable interplay between the structural, chemical, and magnetic properties of molecule-based materials.

In many molecule-based magnets [2], the competing spin-orbit coupling and Jahn-Teller (JT) distortion energies [3] are both important because the orbital angular momentum of a transition-metal ion with a singly-occupied doublet orbital is not quenched by the surrounding crystal field. For a trigonally-distorted crystal field, the low-energy doublet of an Fe(II) ion with filling $3d^6$ is occupied by a single hole, as shown in Fig. 17.1b, and carries an orbital angular momentum L_z^{cf} [4] that can take any value between 0 and 2.

Bimetallic oxalates A[M(II)M'(III)$(ox)_3$] are a versatile class of layered molecule-based magnets with transition metals M(II) and M'(III) arranged in an open honeycomb lattice (sketched in Fig. 17.1a) and coupled by the oxalate bridge ox $= (C_2O_4)^{-2}$ [5,6]. In Fe(II)Fe(III) bimetallic oxalates, every $S = 2$ Fe(II) spin is antiferromagnetically coupled to the three neighboring $S' = 5/2$ Fe(III) spins within each bimetallic layer. While the choice of organic cation A separating the layers does not affect the sign of this exchange interaction, it does shift the orbital-angular momentum L_z^{cf} on the Fe(II) sites. If L_z^{cf} lies between $l_c \approx 0.28$ and 1, the magnetic moments of the Fe(II) and Fe(III) sublattices exactly cancel [7] at a magnetic compensation (MC) temperature $T_{comp} \approx 30\,\mathrm{K}$ [8,9] below the transition temperature $T_c \approx 45\,\mathrm{K}$. When $T < T_{comp}$, these compounds exhibit a metastable state with negative magnetization in small positive fields.

The competition between the spin-orbit and JT energies can produce [10] both upper and lower JT transitions with the open honeycomb lattice distorted by Fe(II) displacements between $T_{\mathrm{JT}}^{(l)}$ and $T_{\mathrm{JT}}^{(u)}$. This paper studies the general relationship between the magnetic and JT transitions in the Fe(II)Fe(III) bimetallic oxalates. For weak enough elastic energies, T_c can lock onto $T_{\mathrm{JT}}^{(l)}$ over a range of L_z^{cf}. For stronger elastic energies, T_c may become double valued with magnetic order suppressed below $T_{\mathrm{JT}}^{(u)}$. In compounds that exhibit MC, $T_{comp} < T_{\mathrm{JT}}^{(l)} < T_c$ and $T_c < T_{\mathrm{JT}}^{(u)}$.

17.2 Model

The crystal field at each Fe site is produced by the six surrounding oxygen atoms, which form two parallel, equilateral triangles rotated by 48° with respect to one another [11]. Because one triangle is bigger than the other, only C_3 symmetry is respected by the trigonally-distorted crystal-field potential. While the $L' = 0$ Fe(III) multiplet is unaffected by the crystal-field potential, the $L = 2$ Fe(II) multiplet splits into two doublets and a singlet [7], as shown in Fig. 17.1b, with the doublet $\psi_{1,2}$ lying an energy Δ below the singlet ψ_3.

Ab initio calculations [10] indicate that $\Delta \gg J_c SS'$ and $\Delta \gg |\lambda|S$, where $\lambda \approx -12.65$ meV is the spin-orbit coupling constant for Fe(II). Consequently, Fe(II) ions carry the non-quenched orbital angular momentum $L_z = \pm L_z^{cf}$, where $0 \leq L_z^{cf} \leq 2$. The choice of cation can alter L_z^{cf} by slightly shifting the position of the Fe(II) atom within the potential landscape produced by the surrounding oxygen atoms.

If the crystal field respected octahedral symmetry, then $L_z^{cf} = 1$ and $\Delta = 0$. The degenerate $\psi_{1,2,3}$ levels would then form the familiar t_{2g} triplet with $L_z = 0$ or ± 1 and the orbital angular momentum $\mathbf{L}$ could be treated as an $L = 1$ operator. But restricted to the orbital doublet $\psi_{1,2}$, the matrix elements $\langle \psi_i | L_\pm | \psi_j \rangle$ ($i, j = 1$ or 2) of the raising and lowering operators $L_\pm = L_x \pm iL_y$ vanish so that the spin-orbit coupling $\lambda L_z S_z = -|\lambda| L_z S_z$ contains no transverse components. Therefore, the orbital angular momentum of the doublet acts like a spin-1/2 Ising variable.

In the absence of spin-orbit coupling, the $S' = 5/2$ Fe(III) moments would always dominate over the $S = 2$ Fe(II) moments. But when the spin-orbit coupling $-|\lambda| L_z S_z$ on the Fe(II) sites is sufficiently strong, the Fe(II) moments will order more rapidly below T_c than the Fe(III) moments. At $T = 0$, the Fe(III) moment again dominates if $S' > S + L_z^{cf}/2$ or $L_z^{cf} < 1$. So MC occurs in a range of L_z^{cf} between l_c and 1.

The Hamiltonian of a non-distorted bimetallic layer is given by

$$H = J_c \sum_{\langle i,j \rangle} \mathbf{S}_i \cdot \mathbf{S}'_j - |\lambda| \sum_i L_i^z S_i^z, \tag{17.1}$$

where $L_i^z = \pm L_z^{cf}$, the $\langle i, j \rangle$ sum runs over all nearest-neighbors, and the i sum runs over all Fe(II) sites. For antiferromagnetic exchange, $J_c > 0$. Based on Eq. 17.1, the appearance of MC in a range of L_z^{cf} between l_c and 1 was verified using hybrid Monte-Carlo simulations [12] with the spins $\mathbf{S}_i$ and $\mathbf{S}'_j$ treated quantum-mechanically and the orbital angular momenta L_i^z treated classically.

Within mean-field (MF) theory, the eigenvalues of $\psi_{1,2;\sigma}$ on the Fe(II) sites are $\varepsilon_{1\sigma} = \varepsilon_{0\sigma} - |\lambda| L_z^{cf} \sigma$ and $\varepsilon_{2\sigma} = \varepsilon_{0\sigma} + |\lambda| L_z^{cf} \sigma$, where $\varepsilon_{0\sigma} = 3J_c M_{S'} \sigma/2$ and $M' = M_{S'} = 2\langle S'_z \rangle$ is the Fe(III) moment with μ_B set to 1. It is then straighforward to evaluate the temperature dependence of $M'(T)$ and of the Fe(II) moment $M(T) = M_S(T) + M_L(T)$, where $M_S = 2\langle S_z \rangle$ and $M_L = \langle L_z \rangle$. Since M and M' always have opposite signs in the absence of an external field, we shall take $M < 0$ and $M' > 0$.

Due to the mixing of the eigenstates $\psi_{1\sigma}$ and $\psi_{2\sigma}$, the JT distortion on the Fe(II) sites is described by the matrix

$$\underline{H}_{\sigma}^{\rm mix} = \begin{pmatrix} \varepsilon_{1\sigma} & \xi \\ \xi & \varepsilon_{2\sigma} \end{pmatrix}, \tag{17.2}$$

where the distortion energy ξ is proportional to the Fe(II) displacement Q. The eigenvalues of $\underline{H}_{\sigma}^{\rm mix}$ are $\varepsilon_{a\sigma} = \varepsilon_{0\sigma} + t_{\sigma}$ and $\varepsilon_{b\sigma} = \varepsilon_{0\sigma} - t_{\sigma}$ where

$$t_{\sigma} = -{\rm sgn}(\sigma)\sqrt{(\lambda L_z^{cf}\sigma)^2 + \xi^2} \tag{17.3}$$

and we define $t_0 = \xi$. Hence, the doublet splitting $2|t_{\sigma}|$ is enhanced by the JT effect (strictly speaking, the pseudo-JT effect when $\varepsilon_{1\sigma} \neq \varepsilon_{2\sigma}$). With the convention that $M' = M_{S'} > 0$, the lowest eigenvalue of $\underline{H}_{\sigma}^{\rm mix}$ is $\varepsilon_{b,-2}$ with $\sigma = -2$.

Including the JT distortion energy ξ, the MF free energy can be written

$$\frac{F}{N} = -T\log\Big\{Z_{\rm II}Z_{\rm III}e^{3J_cM_SM_{S'}/4T}\Big\} + \alpha|\lambda|\left\{\left(\frac{\xi}{|\lambda|}\right)^2 + \gamma_3\left(\frac{\xi}{|\lambda|}\right)^3 + \gamma_4\left(\frac{\xi}{|\lambda|}\right)^4\right\}, \tag{17.4}$$

where

$$Z_{\rm II} = 2\sum_{\sigma} e^{-3J_cM_{S'}\sigma/2T}\cosh\big(t_{\sigma}/T\big), \tag{17.5}$$

$$Z_{\rm III} = 2\sum_{\sigma'} e^{-3J_cM_S\sigma'/2T} \tag{17.6}$$

are the partition functions on the Fe(II) and Fe(III) sites, respectively, containing sums over $\sigma = 0, \pm 1, \pm 2$ and $\sigma' = \pm 1/2, \pm 3/2, \pm 5/2$. The second line in Eq. 17.4 corresponds to the elastic energy proportional to the dimensionless parameter α.

We restrict consideration to displacements $Q \sim \xi$ of the Fe(II) ions either directly into one of the open hexagons or towards one of the neighboring Fe(III) ions, with the former displacements sketched in Fig. 17.1a. The different energy costs for these two types of displacements is reflected in the anharmonic $\gamma_3(\xi/|\lambda|)^3$ term in the elastic energy. Fluctuations between the distorted atomic configurations are assumed to be slow compared with the electronic time scales. The JT distortion is not washed out by an average over the three possible displacements of the Fe(II) ion sketched in Fig. 17.1a because the interactions with other Fe(II) ions will break the threefold symmetry about any site.

It is simple to obtain the equilibrium values for M_S, $M_{S'}$, and ξ from the extremal conditions $\partial F/\partial M_S = \partial F/\partial M_{S'} = \partial F/\partial\xi = 0$. The rather complex expression for the average orbital angular momentum $M_L = \langle L_z\rangle$ on the Fe(II) sites was given in Ref. [10](b).

17.3 Results

Based on the data plotted in Fig. 17.2, Tang et al. [14] attributed two "compensation" temperatures to an Fe(II)Fe(III) compound with cation A = N(n-C_4H_9)$_4$. However, their experimental data is very well described by our model [10] using the parameters $J_c/|\lambda| = 0.037$, $\alpha = 3.7$, $\gamma_3 = -1.9$, $\gamma_4 = 1.1$, and $L_z^{cf} = 0.3$, which is just above the threshold $l_c \approx 0.28$ for MC. Clearly, the upper "compensation" point assigned in Ref.[14] is actually the lower JT transition marked by a jump in the magnetization. The predicted upper JT transition, not shown in Fig. 17.2, should occur at $T_{\rm JT}^{(u)} \approx 0.41|\lambda|$ or about 60 K. Due to the anharmonic term $\sim \xi^3$ in the elastic energy, both predicted lower and upper JT transitions are first order with $\xi \approx 0.8|\lambda|$, corresponding to an atomic displacement of roughly $Q \approx 0.075$ Å.

While the lower JT transition at $T_{\rm JT}^{(l)} \approx 42\,{\rm K} < T_c$ is easy to observe due to the jump in the magnetization, the predicted upper JT transition has not yet been seen. But x-ray measurements [15] on a different sample with the same cation N(n-C_4H_9)$_4$ indicate that the hexagonal symmetry present at room temperature is absent in the monoclinic lattice at 60 K, implying that $60\,{\rm K} < T_{\rm JT}^{(u)} < 290\,{\rm K}$.

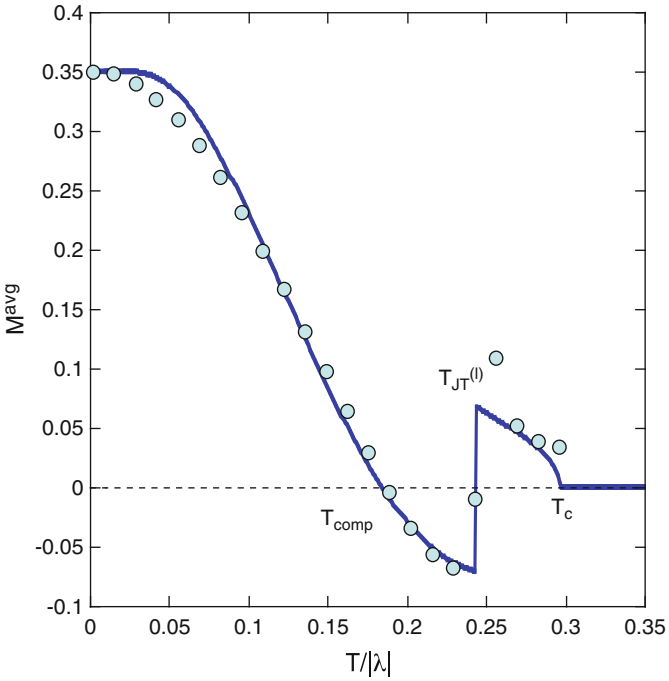

Fig. 17.2 The normalized experimental data [14] (*circles*) for the magnetization of Fe(II)Fe(III) bimetallic oxalate with cation N(n-C_4H_9)$_4$ and the theoretical prediction [10] (*solid curve*) for the average magnetization with $J_c/|\lambda| = 0.037$, $\alpha = 3.7$, $\gamma_3 = -1.9$, $\gamma_4 = 1.1$, and $L_z^{cf} = 0.3$

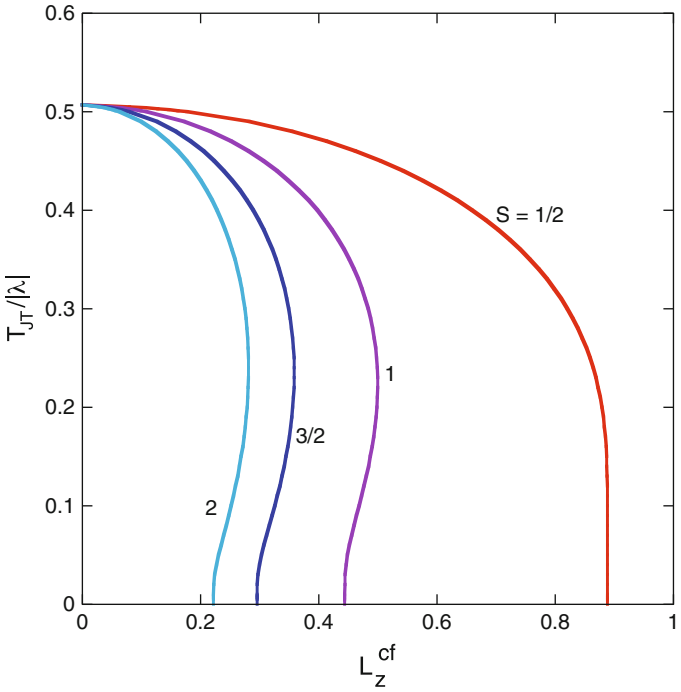

Fig. 17.3 The JT transition temperature versus L_z^{cf} for $\alpha = 4$, $\gamma_3 = -1.9$, $\gamma_4 = 1.1$, $J_c = 0$, and different values of the spin S. $T_{\rm JT}$ can be double valued for ranges of L_z^{cf} when $S > 1/2$

To understand the physical origin of the inverse JT distortion in the Fe(II)Fe(III) bimetallic oxalates, we consider the general problem of a spin-S ion containing a singly-occupied doublet orbital with non-quenched orbital angular momentum L_z^{cf} in the absence of any magnetic coupling ($J_c = 0$). In Fig. 17.3, we plot the JT transition temperature $T_{\rm JT}$ versus L_z^{cf} for $\alpha = 4$, $\gamma_3 = -1.9$, and $\gamma_4 = 1.1$. Notice that $T_{\rm JT}$ depends only on the elastic constants and is independent of S as $L_z^{cf} \to 0$. Both upper and lower JT transitions are found in narrow ranges of L_z^{cf} for $S > 1/2$. This is easy to understand: at low temperatures, the spin states with larger $|S_z|$ and stronger spin-orbit coupling $-|\lambda|L_zS_z$ dominate the free energy and quench the JT distortion.

Although magnetic order is not responsible for the inverse JT transition, it does compete with the JT distortion in interesting ways. Along with the magnetic temperatures T_c and T_{comp}, the JT temperatures $T_{\rm JT}^{(u)}$ and $T_{\rm JT}^{(l)}$ are plotted versus L_z^{cf} in Fig. 17.4 for four different values of the elastic coefficient α. Of course, T_c does not depend on α when $T_c > T_{\rm JT}^{(u)}$ or when the JT transition is absent.

For $\alpha = 2$ or 3, $T_{\rm JT}^{(u)}$ always exceeds T_c, which locks onto $T_{\rm JT}^{(l)}$ over a range of L_z^{cf}, as shown in the insets to Fig. 17.4a,b. Over these ranges of L_z^{cf}, the JT distortion is quenched with the development of long-range magnetic order below T_c.

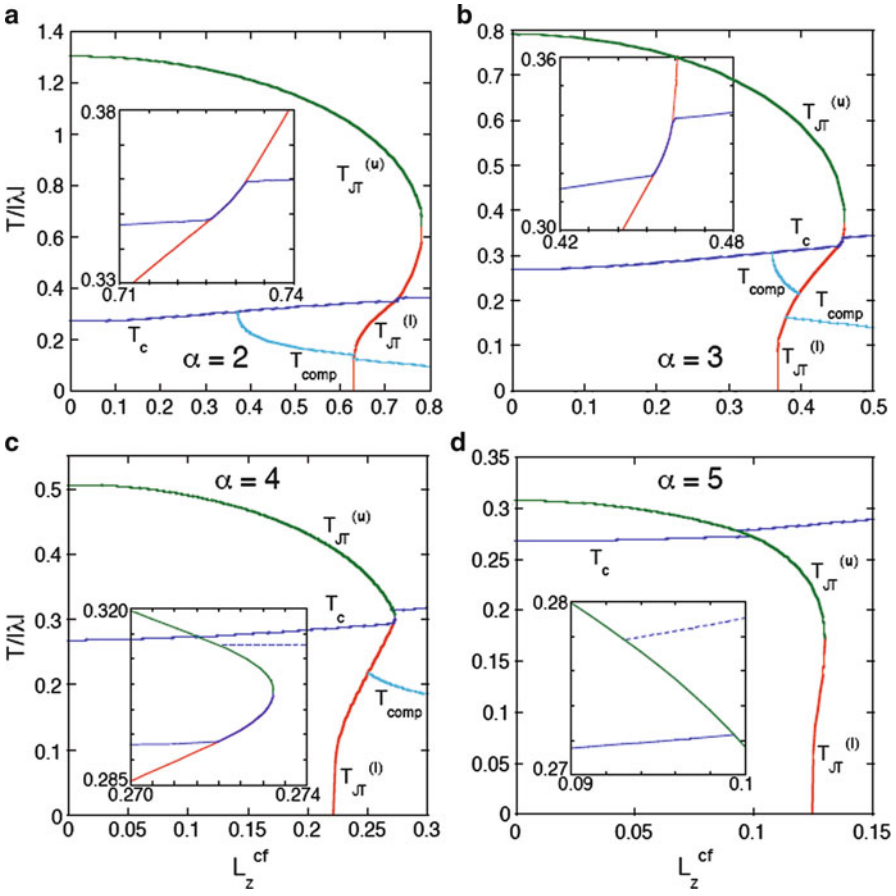

Fig. 17.4 The transition temperature T_c, compensation temperature T_{comp}, and upper and lower JT transition temperatures $T_{\rm JT}^{(l)}$ and $T_{\rm JT}^{(u)}$ versus L_z^{cf} for $\gamma_3 = -1.9$, $\gamma_4 = 1.1$, $J_c/|\lambda| = 0.037$, and $\alpha =$ (a) 2, (b) 3, (c) 4, or (d) 5

For $\alpha = 4$, close to the value of 3.7 used to model the experimental data of Ref.[14], T_c again locks in with $T_{\rm JT}^{(l)}$ up to the point where $T_{\rm JT}^{(u)}$ and $T_{\rm JT}^{(l)}$ meet. But as shown in the inset to Fig. 17.4c, T_c is discontinuous and double valued in the range $0.2721 < L_z^{cf} < 0.2733$. Consequently, magnetic order appears just below the dashed line for the upper T_c, disappears below $T_{\rm JT}^{(u)}$, and then reappears again below the solid curve for the lower T_c, which coincides with $T_{\rm JT}^{(l)}$.

The JT distortion energy ξ and the average magnetization per site $M_{av} = (M + M')/2$ are plotted versus temperature in Fig. 17.5a,b for $\alpha = 4$. A negative value for $M_{av}(T)$ means that the Fe(II) moment $M(T) < 0$ has a larger magnitude than the Fe(III) moment $M'(T) > 0$. As explained above, the JT transition is first order due to the anharmonic term in the elastic energy. For $L_z^{cf} = 0.273, 0.2726$, and

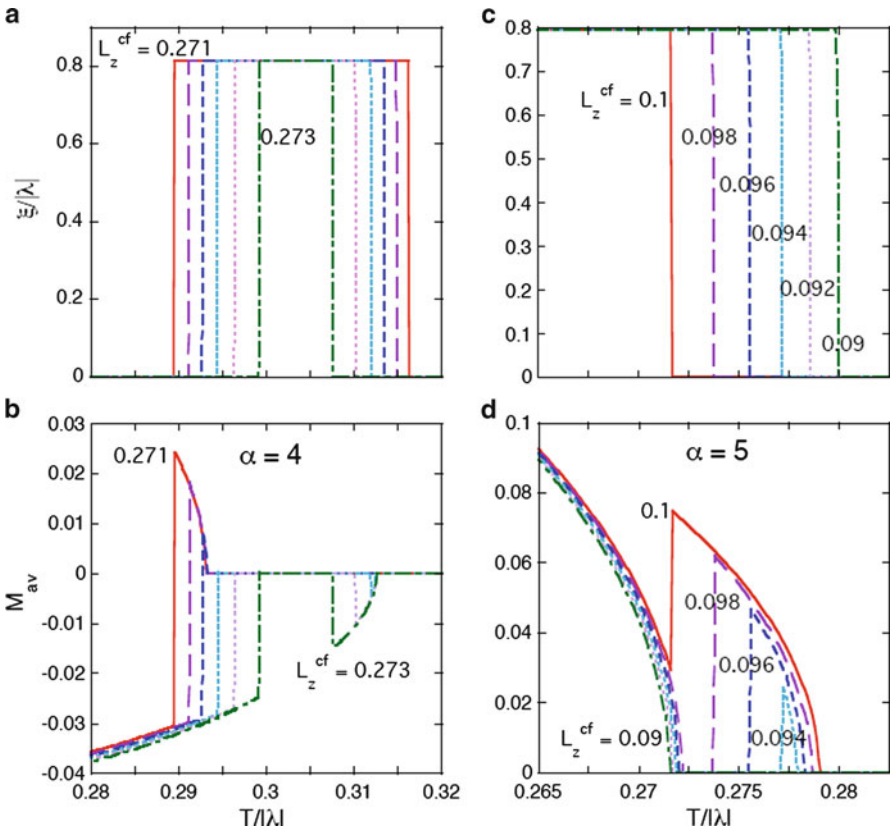

Fig. 17.5 The JT distortion energy ξ (**a, c**) and the average magnetic moment M_{av} (**b, d**) versus temperature for $\alpha = 4$ (**a, b**) or 5 (**c, d**) and several values of L_z^{cf}. Other parameters as in Fig. 17.4

0.2722, the magnetization vanishes when $T_{\rm JT}^{(l)} < T < T_{\rm JT}^{(u)}$ and the lower T_c coincides with $T_{\rm JT}^{(l)}$. For $L_z^{cf} = 0.2718$, 0.2714, and 0.271, the magnetization is positive just below T_c because the magnitude $|M(T)|$ of the Fe(II) moment is suppressed by the JT distortion $\xi \approx 0.81|\lambda|$. Below $T_{\rm JT}^{(l)}$, the average moment changes sign due to the sudden increase in $|M(T)|$. This sign change explains the higher "compensation" point assigned by Tang et al. [14] to the data plotted in Fig. 17.2.

Similar features are seen for $\alpha = 5$ in Fig. 17.4d. Although T_c always exceeds $T_{\rm JT}^{(l)}$, it becomes double valued as it crosses $T_{\rm JT}^{(u)}$. For $0.0932 < L_z^{cf} < 0.0995$, magnetic order appears below the dashed curve for the upper T_c in the inset to Fig. 17.4d, then disappears below $T_{\rm JT}^{(u)}$, and reappears in a first-order transition at the solid curve for the lower T_c. This series of transitions is exhibited in Fig. 17.5c,d. For $L_z^{cf} = 0.09$ and 0.092, the upper JT transition occurs at a higher temperature than the magnetic transition. But for $L_z^{cf} = 0.094$, 0.096, and 0.098, the magnetization first

develops at the upper T_c, is quenched at $T_{\rm JT}^{(u)}$, and then reappears below the lower T_c. For $L_z^{cf} = 0.1$, the average magnetization is suppressed but not quenched at $T_{\rm JT}^{(u)}$.

Since the magnetization can change sign but can not vanish at $T_{\rm JT}^{(l)}$, there is only one compensation temperature for most values of L_z^{cf}. The relation between T_{comp} and $T_{\rm JT}^{(l)}$ is shown in Fig. 17.4. Generally, $M_{av} < 0$ when $T_{comp} < T < T_c$ and $M_{av} > 0$ when $T < T_{comp}$. For $\alpha = 5$, MC only occurs when $L_z^{cf} > 0.234$ so T_{comp} does not appear in Fig. 17.4d. For $\alpha = 4$, $T_{comp} = T_{\rm JT}^{(l)}$ at $L_z^{cf} = 0.251$ and $T_{comp} < T_{\rm JT}^{(l)}$ for $0.251 < L_z^{cf} < 0.273$, above which the JT transition is absent.

But for $\alpha = 2$ and 3, T_{comp} drops when it crosses $T_{\rm JT}^{(l)}$ with increasing L_z^{cf} due to the jump in the magnitude $|M(T)|$ of the Fe(II) moment. As clearly shown in Fig. 17.4b for $\alpha = 3$, two compensation points may lie on either side of an intervening JT transition. In the range $0.38 < L_z^{cf} < 0.397$, M_{av} is negative below T_c, positive between the upper T_{comp} and $T_{\rm JT}^{(l)}$, negative between $T_{\rm JT}^{(l)}$ and the lower T_{comp}, and then positive again at low temperatures.

17.4 Conclusion

The remarkable agreement between experiment and theory in Fig. 17.2 suggests that Fe(II)Fe(III) bimetallic oxalates have an elastic constant $\alpha \approx 3.7$, with qualitatively the same behavior shown in Fig. 17.4c for $\alpha = 4$. For compounds that exhibit MC, Fig. 17.4c implies that $T_{comp} < T_{\rm JT}^{(l)} < T_c$ and $T_c < T_{\rm JT}^{(u)}$. This prediction is substantiated by Nuttall and Day [9], who consistently observed a small jump in the magnetization between T_{comp} and T_c for several Fe(II)Fe(III) compounds with different cations A. The magnetization always jumps to a higher value with increasing temperature because the JT distortion suppresses the magnitude of the Fe(II) moment above $T_{\rm JT}^{(l)}$. Possibly due to a mixture of different stacking patterns for the bimetallic layers [16], the magnetization jumps observed by Nuttall and Day [9] are much smaller than the one observed by Tang et al. [14]. For compounds that do not exhibit MC, it is likely that L_z^{cf} is small enough that $T_{\rm JT}^{(l)} = 0$ ($L_z^{cf} < 0.222$ for $\alpha = 4$). Based on Fig. 17.4c, however, it is possible that $T_{\rm JT}^{(l)} > 0$ even without MC in a narrow window of L_z^{cf} ($0.222 < L_z^{cf} < 0.251$ for $\alpha = 4$).

Whether the pattern of JT displacements is short- or long-ranged depends on the shape and symmetry of the cation that couples the bimetallic layers. Since the cation $N(n\text{-}C_4H_9)_4$ is *not* C_3 symmetric, it may introduce a permanent distortion [10] of the hexagonal lattice at all temperatures. But $N(n\text{-}C_4H_9)_4$ is also just small enough to rotate freely within each unit cell, so it may permit a cooperative, long-ranged JT distortion between $T_{\rm JT}^{(l)}$ and $T_{\rm JT}^{(u)}$. On the other hand, larger cations like $N(n\text{-}C_5H_{11})_4$ will get stuck in different orientations within different unit cells, so that the JT distortion is short-ranged.

To summarize, an inverse JT transition occurs over a narrow range of $L_z^{cf} < 1$ for any ion with spin $S > 1/2$ containing a singly-occupied doublet orbital. In the Fe(II)Fe(III) bimetallic oxalates, magnetic order suppresses the JT distortion and enhances the lower JT transition temperature. Conversely, the JT distortion suppresses and can quench magnetic order below the upper JT transition temperature. A similar range of behavior including first and second-order phase transitions was found by Allen [17] for UO_2. We are hopeful that future x-ray measurements will be able to pinpoint the upper JT transition temperature in the Fe(II)Fe(III) bimetallic oxalates.

Acknowledgments I would like to acknowledge helpful conversations with Dr. Satoshi Okamoto. This research was sponsored by the U.S. Department of Energy, Office of Basic Energy Sciences, Materials Sciences and Engineering Division.

References

1. Miller JS, Epstein AJ (1994) Angew Chem internat edit 33:385; Miller JS, Epstein AJ (2000), MRS Bull. November 21; Miller JS (2002) Adv Mat 14:1105
2. Kahn O (1994) Molecular magnetism. VCH, New York
3. See for example, Bersuker IB (2006) The Jahn–Teller effect. Cambridge University Press, Cambridge, and references therein
4. Palii A, Tsukerblat B, Clemete-Juan JM, Coronado E (2010) Int Rev Phys Chem 29:135
5. Tamaki H, Zhong ZJ, Matsumoto N, Kida S, Koikawa M, Achiwa N, Hashimoto Y, Õkawa H (1992) J Am Chem Soc 114:6974
6. See the review Clément R, Decurtins S, Gruselle M, Train C (2003) Mon für Chem 134:117
7. (a) Fishman RS, Reboredo FA (2007) Phys Rev Lett 99:217203; (b) (2008) Phys Rev B 77:144421
8. (a) Mathonière C, Carling SG, Day P (1994) J Chem Soc Chem Commun 1551; (b) Mathonière C, Nuttall CJ, Carling SG, Day P (1996) Inorg Chem 35:1201
9. Nuttall CJ, Day P (1998) Chem Mat 10:3050
10. (a) Fishman RS, Okamoto S, Reboredo FA (2008) Phys Rev Lett 101:116402; (b) (2009) Polyhedron 28:1740
11. Pellaux R, Schmalle HW, Huber R, Fischer P, Hauss T, Ouladdiaf B, Decurtins S (1997) Inorg Chem 36:2301
12. Henelius P, Fishman RS (2008) Phys Rev B 78:214405
13. (a) Clemente-León M, Coronado E, Galán-Mascarós JR, Gómez-García CJ (1997) Chem Commun 1727; (b) Coronado E, Galán-Mascarós JR, Gómez-García CJ, Ensling J, Gütlich P (2000) Chem Eur J 6:552
14. (a) Tang G, He Y, Liang F, Li S, Huang Y (2007) Physica B 392:337; (b) Bhattacarjee A (2007) Physica B 399:77; (c) Tang G, He Y (2007) Physica B 399:79
15. Watts ID, Carling SG, Day P, Visser D (2005) J Phys Chem Sol 66:932
16. Nuttall CJ, Day P (1999) J Solid State Chem 147:3
17. Allen SJ (1968) Phys Rev B 167:492